Mater. Res. Soc. Symp. Proc. Vol. 928 © 2006 Materials Research Society 0928-GG16-03

Preparation and Characterization of Solid Oxide Fuel Cells Cathode Films

Laura Baqué[1,2], Adriana Serquis[1,2], Nicolás Grunbaum[1], Fernando Prado[1,2], and Alberto Caneiro[1,2]
[1]Instituto Balseiro - Centro Atomico Bariloche, Bariloche, 8400, Argentina
[2]CONICET, Bariloche, 8400, Argentina

ABSTRACT

Perovskite oxide cobaltites with composition $La_{0.4}Sr_{0.6}Co_{0.8}Fe_{0.2}O_{3-\delta}$ were prepared by an acetic acid-based gel route. Then, cathodes were deposited onto porous ceramic substrates, like the usual electrolytes Cerium Gadolinium Oxide (CGO), by spray, spin coating and dip-coating. The structure and morphology of the layers were characterized by XRD and SEM, respectively. Electrical properties were characterized by complex impedance measurements. The correlation between structural characteristics and electrical properties is discussed.

INTRODUCTION

In recent years, perovskite oxide mixed conductors (La, Sr)$MO_{3-\delta}$ (M= transition metal) have attracted much attention because of their potential applications, including oxygen separation membranes and solid oxide fuel cell (SOFC) cathodes. The electronic conductor (La, Sr)$MnO_{3-\delta}$ (LSM) is widely used in commercial SOFC at temperatures higher than 900°C. A decrease of working temperature of SOFCs, in the range of 600–800 °C, is necessary to allow both the use of cost-effective interconnects and the decrease in the thermal degradation of cells. However, in this range of temperature, SOFCs performances are principally limited by cathode overpotential. Even if the influence of cathode film microstructure was recognized to be a key parameter, most of studies have just dealt with the influence of cathode film composition. One proposed solution was to add an ionically conducting second phase to the electronically conducting electrode material. For example, yttria-stabilized zirconia YSZ is often mixed with strontium-doped lanthanum manganite LSM, resulting in polarization resistance values significantly lower than single-phase LSM cathodes [1-3]. Other composite cathodes consisting of LSM and $Ce_{0.8}Gd_{0.2}O_{2-\delta}$ (GDC) on yttria-stabilized zirconia YSZ and GDC electrolytes were also reported [4].

On the other hand, the cobaltites $La_{1-x}Sr_xCo_{1-y}Fe_yO_{3-\delta}$ (LSCF) are good candidates for SOFC cathodes because these materials present high ionic and electronic conductivity, allowing a lower temperature of operation [5,6]. Therefore, efforts have to be done on the synthesis processes of these materials in order to prepare cathodes with different microstructures. In the literature, most of the composite films have been synthesized by the slurry deposition techniques such as spraying [7], painting [8], or spin coating [4,9]. In order to increase SOFCs performances further, it is necessary to understand how the microstructure of the composites electrodes affects the performance of the system.

The aim of this work is to study the electrode resistance of porous electrodes of the same composition films ($La_{0.4}Sr_{0.6}Co_{0.8}Fe_{0.2}O_{3-\delta}$) deposited by different methods and to identify the

sintering conditions to obtain lower cathode overpotential than conventional LSM at low temperatures. The influence of the microstructure on the transport properties (ionic and electronic conductivity) is evaluated by means of impedance spectroscopy.

EXPERIMENTAL DETAILS

$La_{0.4}Sr_{0.6}Co_{0.8}Fe_{0.2}O_{3-\delta}$ powder samples were prepared by an acetic acid-based gel route [10]. More details were reported elsewhere [7]. The resulting powder was fired at 800 °C during 6 h in air. The ink for electrode deposition was prepared mixing the as prepared powder with ethanol, terpineol, polyvinyl butyral, and polyvinyl pyrridone in appropriate ratio. The electrolyte $Ce_{0.9}Gd_{0.1}O_{2-\delta}$ (CGO) was prepared by pressing pellets of commercial powder (Praxair) into 12.5 mm diameter discs, 1 mm thick and firing them at 1350 °C during 12 h in air. Both sides of the electrolyte were rectified before depositing the cathode ink on them by spraying, dip coating or spin coating. Afterwards these assemblies were heat treated at the sintering temperature (see Table I) for 6 h in air to reach a sufficient adherence between electrodes and electrolyte.

The formation of the perovskite phase was verified by means of powder X-ray diffraction (XRD) measurements ($10º \leq 2\theta \leq 70°$) by using a Philips PW1700 diffractometer with Cu–Kα radiation and a graphite monochromator. The thickness and morphology of the electrodes were determined with a Philips 515 scanning electron microscopy (SEM).
Impedance spectroscopy measurements were carried out on heating from 550 to 800 °C in air or over oxygen partial pressures ranging from 10^{-3} to 1 atm, by steps of 50 °C, by using a potentiostat/impedance analyzer Autolab (Eco Chemie BV) between 10^{-3} and 10^{4} Hz. The electrochemical cell was prepared with the symmetrical configuration and platinum grids, slightly pressed on porous electrodes, were used as current collectors.

RESULTS and DISCUSSION

Microstructural characterization

The cross-sectional SEM images corresponding to cathodes prepared by dip coating (cathode *a* – fig. 1.*a*), spray (cathode *b* – fig, 1.*b*) and spin coating (cathode *c* – fig. 1.*c*) are shown in figure 1. LSCF cathode is placed on the top and CGO electrolyte at the bottom in all

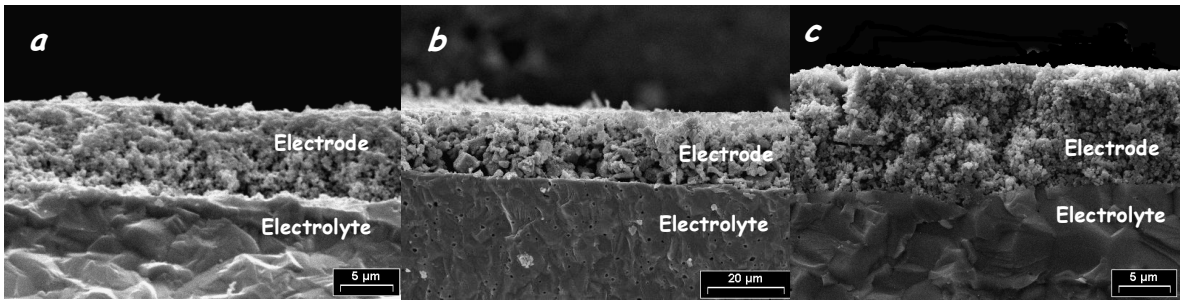

Figure 1. Cross-sectional SEM images of (*a*) cathode a, (*b*) cathode b and (*c*) cathode c.

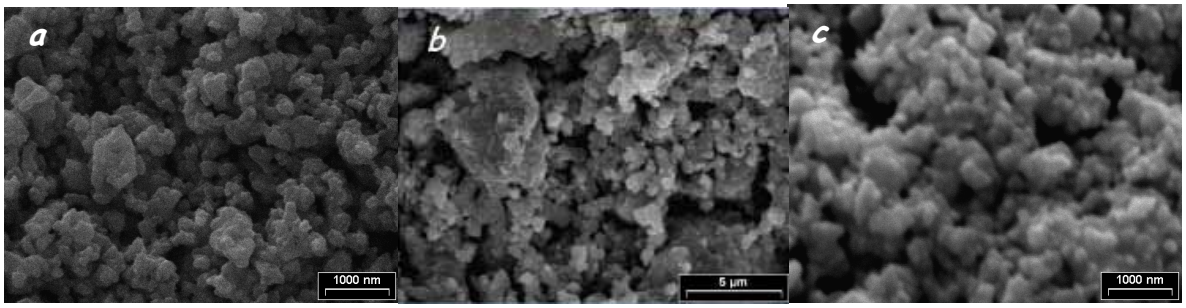

Figure 2. Surface SEM images of (*a*) cathode a, (*b*) cathode b and (*c*) cathode c.

cases. It is possible to observe that all cathodes exhibit a different porous distribution. Thickness for cathode *a*, *b* and *c* are summarized in table I.

Figure 2 shows the surface SEM images of cathode *a* (Figure 2.*a*) and *c* (Figure 2.*c*), and cross-section image of cathode *b* (Figure 2.*b*). The difference in particle sizes between the sprayed cathode and the others due to the final sintering temperature is clearly observed. Particle sizes measured from these images are summarized in table I.

X-ray diffraction patterns of cathode *a* and *b* are displayed in figure 3. The XRD pattern of cathode *c* is similar to cathode *a* and was not included in this figure. Only reflections corresponding to LSCF perovskite phase (R-3c space group) [6] and $Ce_{0,1}Gd_{0,9}O_{2-\delta}$ fluorite phase (Fm3m space group) [12] are present, suggesting that there was no chemical reaction between LSCF and CGO. In the inset are expanded three peaks corresponding to LSCF phase ($2\Theta = 53º$), CGO phase ($2\Theta = 56º$) and the overlap of LSCF and CGO phase ($2\Theta = 59º$). The peak corresponding to LSCF phase of cathode *a* (deposited by dip coating) is wider than the peak corresponding to LSCF phase of cathode *b* (deposited by spray). This result agrees with the SEM observations and indicates that cathode *a* has smaller crystallite size than cathode *b*. Crystallite sizes estimated by Scherer formula [13] are summarized in table I. Table I summarizes the values of thickness and particle size determined by SEM, crystallite size determined by XRD and the sintering temperature of cathodes *a*, *b* and *c*. Crystallite sizes are smaller than particle sizes, which means that particles observed by SEM contains several single crystalline grains. Crystallite and particle sizes obtained by dip and spin coating are smaller than those obtained by spray because it is possible to obtain good adherence with lower sintering temperatures than sprayed films. The relation between sintering temperatures and crystallite sizes is under study.

Table I. Particle size and thickness determined by SEM, crystallite size determined by XRD and sintering temperature of cathode *a*, *b* and *c*.

Cathode	Particle size SEM	Crystallite size XRD	Thickness	Sintering temperature
***a* (dip-coating)**	180 nm	50 nm	9.1 µm	900 ºC
***b* (spraying)**	600 nm	250 nm	20 µm	1000 ºC
***c* (spin-coating)**	160 nm	40 nm	12.4 µm	900 ºC

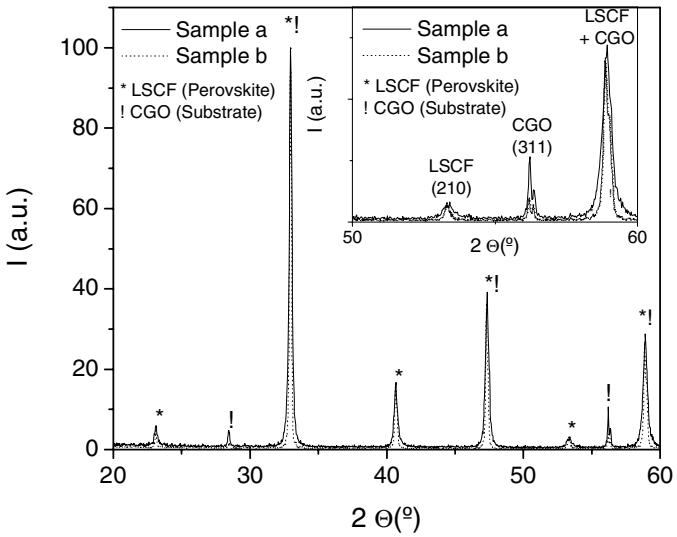

Figure 3. X-ray diffraction pattern of cathode a (—) and cathode b (…).

Electrochemical characterization

In figure 4 are shown the complex impedance spectra in air at 750 ºC of cathodes *a* (deposited by dip coating), *b* (deposited by spray) and *c* (deposited by spin coating). Polarization resistance of cathode *b* is at least one order of magnitude higher than polarization resistance of cathodes *a* and *c* for all measured temperatures (from 600 ºC to 800 ºC). This difference is much larger than the expected for the electrode resistance dependence with thickness [7].

Arrhenius plot of area specific resistance (ASR) of our samples and other cathodes reported in literature [8,9] are plotted in figure 5(a). Table II summarizes ASR and activation

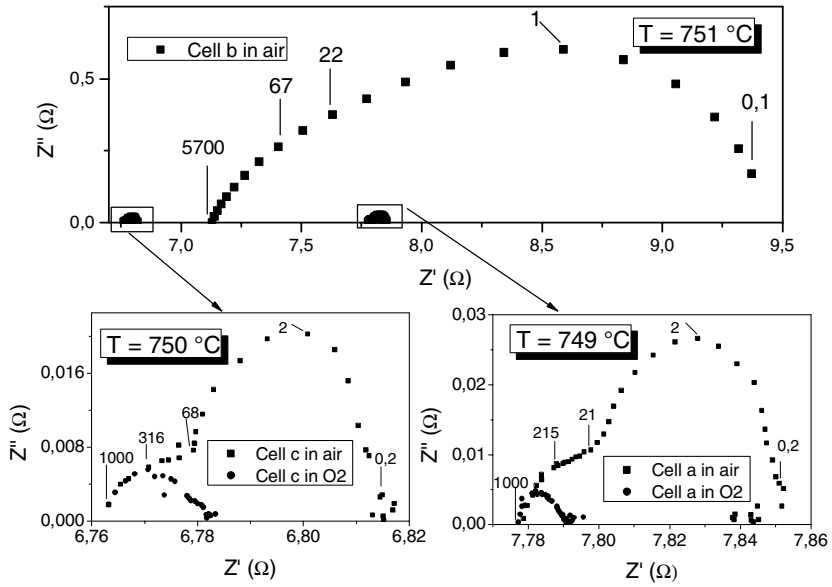

Figure 4. Complex impedance spectra in air at 750 ºC of cathodes *a*, *b* and *c*.

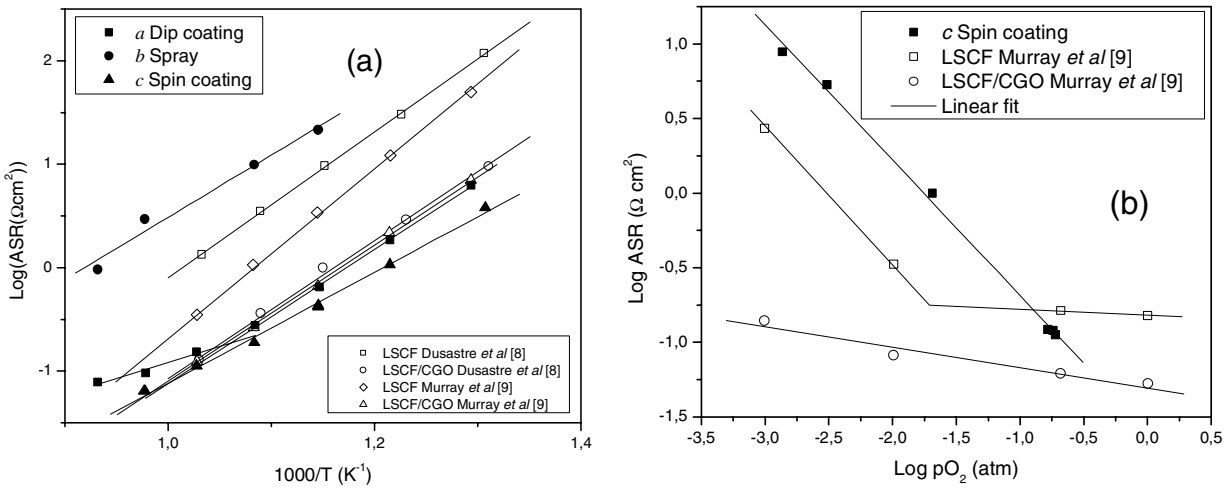

Figure 5. (a) Arrhenius plot for cathodes *a*, *b* and *c*. (b) Oxygen partial pressure dependence of polarization resistance of cathode *c*. Literature results are also included (see Refs. [8,9])

energy values (Ea) of these cathodes. Ea values were calculated from the Arrhenius plot slopes using a linear fit. Two different slopes are observed in the case of the cathode deposited by dip coating (cathode *a*). This would indicate a change with temperature in the limiting mechanisms governing the cathode reaction. The origin of such behavior and possible limiting mechanisms of oxygen reaction are being investigated. ASR and Ea values of cathode *a* are lower than those reported in literature for LSCF cathodes. In addition, ASR values at low temperatures are in agreement with those reported in the literature for LSCF/CGO composite cathodes, but they are higher at high temperature due to the lower activation energy. Electrochemical properties (ASR and Ea) have the lowest values for samples prepared by spin coating (even compared to other works).

The dependence of ASR with oxygen partial pressure at 750 ºC is shown in figure 5(b) for cathode *c*. Similar data reported by Murray *et al* [9] is included for comparison (see table II). ASR values of cathode *c* are smaller than those of Murray LSCF cathode for partial oxygen

Table II. ASR and Ea values of cathodes *a*, *b* and *c* and cathodes reported in the literature.

Cathode	Electrolyte	Method	Ea (eV)	Ref.
$La_{0,4}Sr_{0,6}Co_{0,2}Fe_{0,8}O_{3-\delta}$	$Ce_{0.9}Gd_{0.1}O_{2-\delta}$	Dip coating	0.61 1.29	This work
		Spray	1.20	
		Spin coating	1.03	
$La_{0,6}Sr_{0,4}Co_{0,2}Fe_{0,8}O_{3-\delta}$	ZrO_2:Y_2O_3	Spin Coating	1.65	[9]
$La_{0,6}Sr_{0,4}Co_{0,2}Fe_{0,8}O_{3-\delta}$ + 60%wt $Ce_{0.8}Gd_{0.2}O_{2-\delta}$			1.30	
$La_{0,6}Sr_{0,4}Co_{0,2}Fe_{0,8}O_{3-\delta}$	$Ce_{0.9}Gd_{0.1}O_{2-\delta}$	Slurry painting	1.4	[8]
$La_{0,6}Sr_{0,4}Co_{0,2}Fe_{0,8}O_{3-\delta}$ + 70%wt $Ce_{0.9}Gd_{0.1}O_{2-\delta}$			1.31	
$La_{0,9}Sr_{0,1}MnO_{3-\delta}$	ZrO_2:Y_2O_3		1.9	[11]

pressure close to the air, while they are higher for low partial pressure. This is owned to the fact that the plot slope corresponding to cathode *c* is similar to the LSCF cathode reported by Murray for low partial oxygen pressure. ASR and slope values are higher than those of Murray LSCF/CGO cathode. Plot slope corresponding to cathode *c* is equal to -0.9, indicating a strong dependence of this cathode performance with oxygen partial pressure, due to a process limited by the internal diffusion of oxygen through the oxide layer. It could be due to a high porosity, but it must be investigated.

SUMMARY

In summary, electrochemical properties of LSFC cathodes films strongly depend on the microstructure that is mainly determined by synthesis parameters and technique used for the deposition of the films. Spray films have larger grains than the other techniques because they need larger temperatures to obtain good adherence. As a consequence, this sample presents the larger ASR values. The activation energy values of all the cathodes are lower than those reported in the literature for similar cathode compositions. Besides, both ASR and Ea have the lowest values for samples prepared by spin coating.

ACKNOWLEDGMENTS

The authors acknowledge the financial support of CONICET, Fundación Antorchas, Cooperation Program ECOS-SUD and SECYT – PICT.

REFERENCES

1. T. Tsai, S.A. Barnett, *Solid State Ionics* **93**, 207 (1997).
2. C.W. Tanner, K.-Z. Fung, A.V. Virkar, *J. Electrochem. Soc.* **144**, 21 (1997).
3. M. Gaudon, C. Laberty-Robert, F. Ansart, P. Stevens, A. Rousset, *Solid State Sciences* **5**, 1377 (2003).
4. E. P. Murray, T. Tsai, S.A. Barnett, *Solid State Ionics* **110**, 235 (1998).
5. Y. Teraoka et al, *Mater. Res. Bull.* **23**, 51 (1988).
6. F. Prado, N. Grunbaum, A. Caneiro, A. Manthiram, *Solid State Ionics* **167**, 147 (2004).
7. N. Grunbaum, L. Dessemond, J. Fouletier, F. Prado, A. Caneiro, *Solid State Ionics* **177**, 907 (2006).
8. V. Dusastre, and J. A. Kilner, *Solid State Ionics* **126**, 163 (1999).
9. E. P. Murray, M. J. Sever and S. A. Barnett, *Solid State Ionics* **148**, 148 (2002).
10. Y. Xia, T. Armstrong, F. Prado, A. Manthiram, *Solid State Ionics* **130**, 81 (2000).
11. E. Siebert, A. Hammouche, and M. Kleitz, *Electrochemica Acta*, **40**, 1741 (1995).
12. G. Corbel, S. Mestiri, and P. Lacorre, *Solid State Science* **7**, 1216 (2005).
13. G. L. Clark, Applied X Rays, 4 ed (Mc Graw Hill, 1995).